

Finite Size Effect in Amorphous Indium oxide

Sreemanta Mitra^{‡,*}, Girish C Tewari, Diana Mahalu, and Dan Shaha[†]

Department of Condensed Matter Physics, The Weizmann Institute of Science, 76100 Rehovot, Israel[‡]

We study the low temperature magneto-transport properties of several highly disordered amorphous Indium oxide(a:InO) samples. Simultaneously fabricated devices comprising a 2-dimensional (2D) film and 10 μm long wires of different widths were measured to investigate the effect of size as we approach the 1D limit, which is around 4 times the correlation length, and happens to be around 100 nm for a:InO. The film and the wires showed magnetic field (B) induced superconductor to insulator transition (SIT). In the superconducting side, the resistance increased with decrease in wire width, whereas, an opposite trend is observed in the insulating side. We find that this effect can be explained in light of charge-vortex duality picture of the SIT. Resistance of the 2D film follows an activated behavior over the temperature (T), whereas, the wires show a crossover from the high- T activated to a T -independent behavior. At high temperature regime the wires' resistance follow the film's until they deviate and became independent of T . We find that temperature at which this deviation occurs evolve with magnetic field and the width of the wire, which show the effect of finite size on the transport.

PACS numbers: 73.63.-b, 05.30.Rt

I. INTRODUCTION

Quantum phase transition (QPT)^{1,2}, an important paradigm of condensed matter physics, continues to generate immense experimental and theoretical interest. These transitions are accompanied by quantum rather than thermal fluctuations - where change in a parameter in the Hamiltonian of the system induces a transition from one ground state to another fundamentally different ground state³. Superconductor to insulator transition (SIT) is an archetypal QPT, which can be tuned by disorder⁴, electric field⁵ or magnetic field (B)⁶. Although defined strictly at the absolute zero of temperature ($T=0$), SIT has dramatic manifestations at experimentally accessible T s. SIT has been studied in several two-dimensional (2D) systems⁷, from highly disordered superconductors⁸⁻¹⁰ to high- T_C superconductors¹¹. Despite difficulties in fabrication, SIT has also been studied in several quasi-1D systems¹²⁻¹⁵. Amorphous InO was also studied in quasi 1D form¹⁶ with width ranging from 40 to 100 nm. Some of the wires showed vanishing resistance as T is approached to zero below superconducting critical T (T_C) and some saturated at a non-zero value ranging from 0.06-40 k Ω . Below T_C , the magnetoresistance showed reproducible oscillations, which are reminiscent to that of superconducting interference device. The existence of superconductivity in the high disorder limit becomes more intriguing when the applied B induces vortices, which remain mobile at any finite T due to the presence of disorder and a true superconducting state, where the vortices are localized can only be achieved at $T=0$.

One of the central issues in the 2D SIT, is the nature of conduction in the insulating state of B tuned SIT, where at low- T resistance per square (R_{\square}) become very high^{17,18}. In several 2D disordered superconductors, such as thin MoGe films¹⁹, Ta films²⁰, amorphous Bi films²¹ (R_{\square}) become independent of T as the low-

est T is approached. It was thought that formation of metallic state or macroscopic quantum mechanical tunneling of the vortices lead to this T independence of R_{\square} ^{9,19,22}. Weakening of the cooling of charge carriers by the phonon bath due to weak electron-phonon coupling can also lead to T independent R_{\square} . Microwave spectroscopy on amorphous Indium oxide films²³ provides evidence of B -induced metallic state in the superconductor to insulator transition, where a crossover from superconductor to metallic state occurs at much lower B than the conventional crossover. In case of going from 2D to quasi-1D system, several new features were observed. T_C is reduced in case of amorphous MoGe films²⁴ as the width is reduced and superconductivity was completely destroyed in the 1D limit. A recent work suggested that T_C decreases exponentially with the inverse of wires' cross sectional area²⁵. The wires studied here are not 1D in strict sense, as per dimension is concerned, our only aim here is to see how the finite size affects the transport properties as we move down to the 1D limit. Intuitively we expect that, if we reduce the width, R_{\square} should increase. The as-prepared insulating wires' R_{\square} increase with reduction of width (w), however, a counterintuitive trend is observed in the insulating side for the wires going through a B -driven SIT. In the insulator side of SIT, wires' R_{\square} increase with w .

In this Paper, we aim to address this puzzle by a detailed systematic size dependent investigation of magnetotransport measurements in a:InO devices.

II. EXPERIMENT

The results which we present here are from 10 μm long wires with three different w , 0.1, 0.2 and 0.4 μm . The devices were initially defined by e-beam lithography on a Si/SiO₂ substrate and then 25 nm a:InO was electron-gun evaporated from ultrahigh pure sintered In₂O₃ targets in

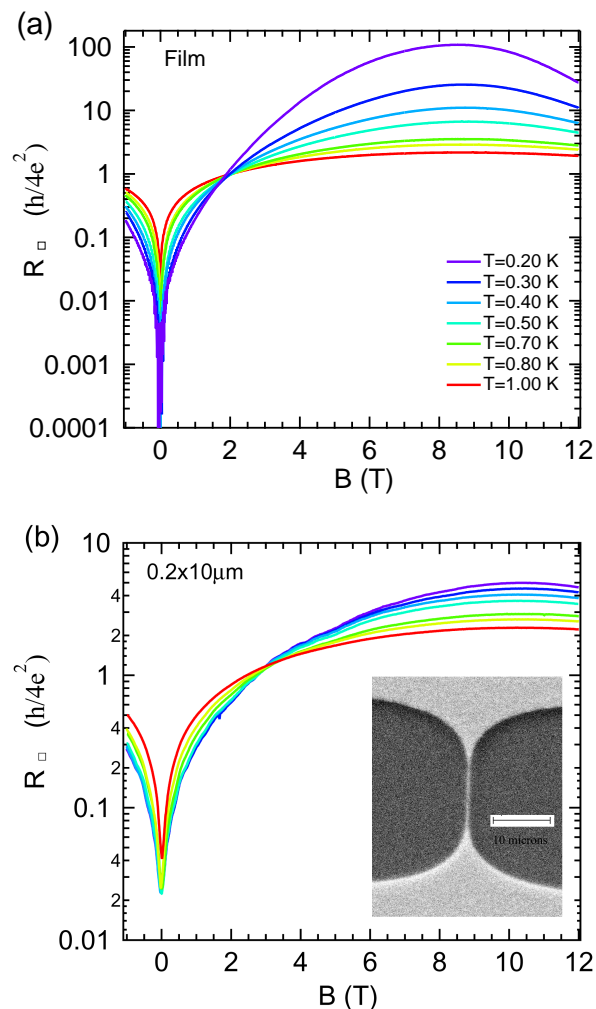


FIG. 1. (a) The R_{\square} vs B isotherms (in semi-log scale) for the film, showing B -driven SIT ($B_c \cong 2.07$ T). The R_{\square} scale is shown in the unit of quantum resistance of Cooper pair ($R_Q = h/(2e)^2$). The critical resistance (R_c) is almost equal to R_Q . (b) The $R_{\square}(B)$ isotherms for $w=0.2 \mu\text{m}$ wire in a semi-log plot. The critical magnetic field, B_c is 3.03 T. At B_c , the resistance is $1.18R_Q$. Same color legends for same T as (a) is used. (Inset: Scanning electron microscopy image of a 10 μm long wire.)

an oxygen atmosphere of residual pressure 1.5×10^{-5} Torr. Apart from these wire devices, we prepare a film of size $50 \times 165 \mu\text{m}$, simultaneously under the same condition to observe the finite size effect on electronic transport, for a:InO, as we reduce the width. All devices, wires and film, were patterned on a single chip and fabricated simultaneously. The patterns were transferred using lift-off process. For transport measurements, gold contact pads were prepared by optical lithography followed by thermal evaporation and lift-off. The wires and the film of a:InO form a bridge between the contact pads. The chip was mounted on a chip carrier, and $25 \mu\text{m}$ Au wires were used to bond for electrical connections between the de-

vices and chip carrier gold pad. The inset of Figure 1(b) shows the scanning electron microscopy image of a wire, used for the transport measurements.

The devices were cooled in a dilution refrigerator and magneto-transport measurements were performed using standard low frequency ac lock-in technique in two-terminal configuration. The measurements were done in a current bias condition, with an applied bias $I_{ac}=1$ nA, which is well within the Ohmic regime. The signal from the sample was amplified by a home made differential pre-amplifier and measured using lock-in amplifiers. All the devices studied in the present work, a particular trend in the experimental result is observed and its not random in anyway. The magneto-transport isotherms were also found to be in appropriate way as observed previously in numerous occasions and follow the theoretical arguments perfectly. This systematics of the data suggested that heating or external noise has no significant effect on the measurements. Magnetic field up to 12 T was applied perpendicular to the surface of the devices. Resistance mentioned here is the resistance per square, R_{\square} . At room- T , and $B=0$ T, the film's R_{\square} is ~ 1.4 k Ω . The wires' R_{\square} , on the other hand, varies between 2.6-2.8 k Ω . Prior to determine the R_{\square} , the contact resistance ($\sim 490 \Omega$) was subtracted. The subtracted resistance value was then normalized with the number of squares in series (*e.g.* $0.1 \mu\text{m}$ wide wire has 100 squares) to get R_{\square} . The contacts are identical for all the devices, and most of the contact resistance originated from the connecting wires on the probe.

III. RESULTS AND DISCUSSION

We begin to present our findings by showing $R_{\square}(B)$ isotherms obtained from our devices. Figure 1(a) and (b) show $R_{\square}(B, T)$ of the film and $0.2 \mu\text{m}$ wide wire respectively. The R_{\square} values are given in the unit of quantum resistance of Cooper pair ($R_Q = h/(2e)^2 = 6.45$ k Ω). Similar data have been obtained from the wires with $w=0.1$ and $0.4 \mu\text{m}$. The isotherms as shown in Figure 1, cross each other at particular B , B_c , signifying B -driven SIT. The critical R_{\square} , (R_{\square} value at B_c) R_c , for the film is close to R_Q ($1 \pm 0.05 R_Q$), which suggests a phase transition driven by quantum phase fluctuations and Cooper pair (de)localization expected within the bosonic description of SIT²⁶. For the wires, R_c is not very different from R_Q ; *e.g.* $R_c = 1.18R_Q$ for $w=0.2 \mu\text{m}$ wire. The values of the parameters for all the devices studied are summarized in Table I.

To look at the nature of transport on both sides of the SIT, we plot the T dependence of R_{\square} for various B values. The data were extracted from the $R_{\square}(B)$ isotherms obtained for the Film and the $0.2 \mu\text{m}$ wire as shown earlier in Figure 1. Figure 2(a) shows an Arrhenius plot of R_{\square} for 6 different ($\frac{B}{B_c}$) values ranging from the superconducting to the insulating state for the film. At $B=0$, $(R_{\square})_{Film}$ decreases and appeared to go to zero as

TABLE I. List of parameters for all the devices. The R_{\square} values are given in terms of quantum resistance of Cooper pair ($R_Q = h/(2e)^2 = 6.45 \text{ k}\Omega$). RT stands for room temperature.

Device	R_{\square} (RT)	$B_c(T)$	R_c	R_{\square}^{peak} (1.0 K)	R_{\square}^{peak} (0.2 K)
2D Film	$0.217R_Q$	2.07	$1.0 \pm 0.05R_Q$	$2.17R_Q$	$107.8R_Q$
$0.40 \mu\text{m}$ wire	$0.434R_Q$	7.20	$1.58 \pm 0.07R_Q$	$1.98R_Q$	$3.68R_Q$
$0.20 \mu\text{m}$ wire	$0.403R_Q$	3.03	$1.18 \pm 0.08R_Q$	$2.28R_Q$	$4.98R_Q$
$0.10 \mu\text{m}$ wire	$0.418R_Q$	1.30	$0.92 \pm 0.06R_Q$	$2.83R_Q$	$6.73R_Q$

T is decreased, signifying superconducting ground state. For the wires, on the other hand, R_{\square} saturate as T is decreased. For ($\frac{B}{B_c} < 1$), R_{\square} drops as T is decreased, following,

$$R = R_0 \exp\left(-\frac{T_0}{k_B T}\right) \quad (1)$$

where, T_0 is the activation energy, k_B is the Boltzmann constant and R_0 is a pre exponential normalization factor. Increasing the magnetic field, increases the low- T limit of R_{\square} . In the superconducting side, for nonzero B , R_{\square} deviated from the high- T activated behavior as T is lowered and tend to become independent of T . It was thought that, near SIT, disordered superconducting films may intrinsically break up into islands, which might be the reason behind this T independence of R_{\square} at low- T s^{27,28}. In the insulating side, above B_c , no such deviation is observed and R_{\square} increases rapidly as a function of $(1/T)$ over the full dynamic range. This behavior can be fitted with the activated form described in Equation 1. In Figure 2(b), we show similar Arrhenius plots for the $0.2 \mu\text{m}$ wide wire, for the same ($\frac{B}{B_c}$) values as in Figure. 2(a). The data clearly show a crossover from the high- T activated behavior to a leveling of R_{\square} at low- T s. Similar behavior has been observed for the other wires studied here. At zero- B , this leveling might be suggestive of phase-slip processes²⁹. At non-zero B , this crossover to a T -independent state might indicate that the system change from activated to a metallic dissipative state²². Another effect that would cause this tendency of the resistance to flatten at low- T is thermal decoupling of the electrons from the phonon bath, but this is more likely to occur at much lower T ^{30,31} than 0.8 K , where it is actually seen in this study. It was argued in ref.²² that this leveling of resistance at low T possibly originates from a macroscopic quantum mechanical tunneling of vortices between pinning sites, where the tunneling objects are dislocations and antidislocations of the vortex lattice. Also a model^{32,33} for crossover from a vortex solid phase to a quantum vortex liquid phase suggests temperature independent R_{\square} at low- T . Although the isotherms for the film and the $0.2 \mu\text{m}$ wide wire look similar in appearance, and R_{\square} increases with B until it reaches a magnetoresistance peak in the insulating side, there are significant differences. In the superconducting side of the SIT, the wire has higher R_{\square} than the film. At

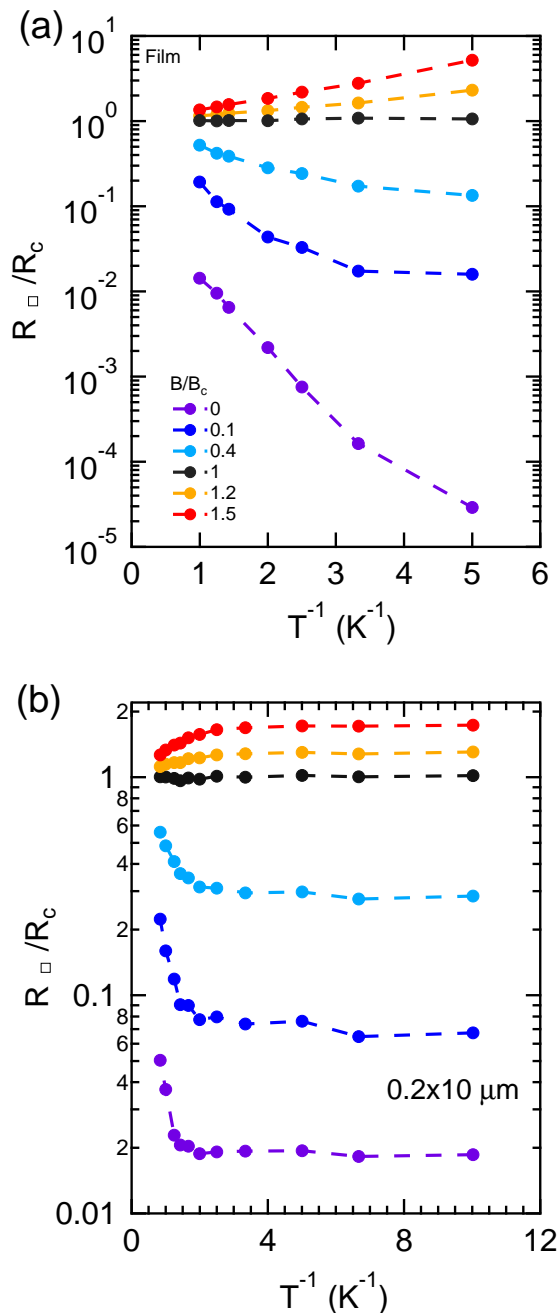


FIG. 2. (a) Arrhenius plot of R_{\square} (normalized with respect to R_c) of the film for six different ($\frac{B}{B_c}$) values. (b) Similar plot of R_{\square} of the $w=0.2 \mu\text{m}$ wire for the same ($\frac{B}{B_c}$) values as (a). Same color scheme has been used in both the figures. The dashed lines joining the data points are to guide the eye. The wire's R_{\square} show a crossover from the high- T activated to a T independent behavior as T is lowered.

high- T , R_{\square} of the film is of the same order of magnitude as wire [see Figure 3]. However, the film's R_{\square} increases faster with B , giving rise to order of magnitude higher R_{\square} in the insulating state at low T .

This is seen more clearly when we plot in Figure 4(a)

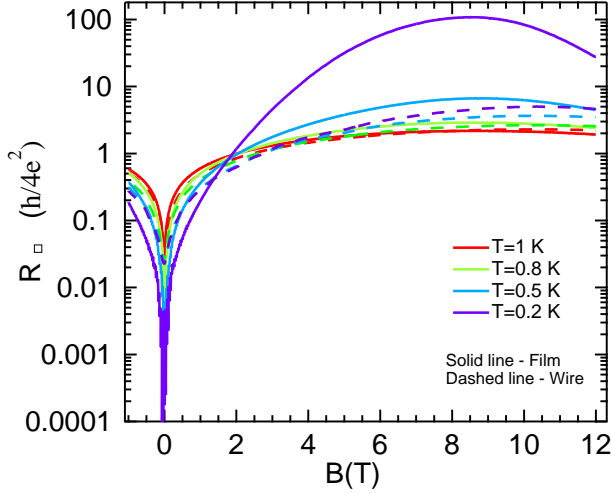


FIG. 3. $R_{\square}(B)$ isotherms for both film and $0.2 \mu\text{m}$ wire, at 4 different T s. Same color has been used for same temperature. The solid and dashed lines are for the film and the wire respectively. For the lowest T shown, $(R_{\square})_{\text{Film}}$ is order of magnitude higher than $(R_{\square})_{\text{wire}}$, in the insulating side.

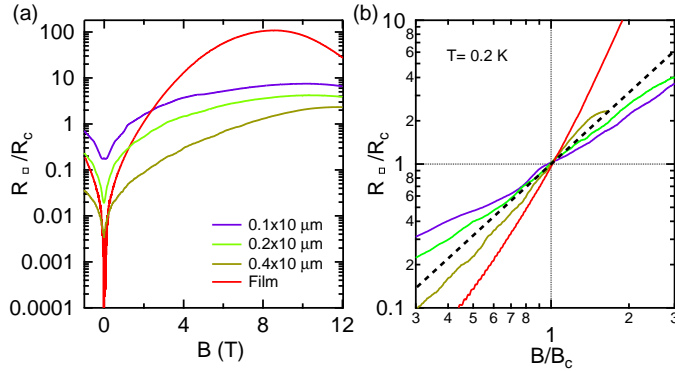


FIG. 4. (a) $R_{\square}(B)$ for all the wires along with the film measured at $T=0.2 \text{ K}$. The resistance values are normalized with respect to respective R_c of the devices. (b) The $R_{\square}(B)$ for the same devices measured at 0.2 K , shown in double-logarithmic plot. The B scale is normalized with respect to respective B_c values. The linearity in double logarithmic plot near $(\frac{B}{B_c}=1)$, suggests power law behavior. A dashed straight line is drawn to guide the eye. The linear behavior extends deep in to the insulating side, suggests that vortex transport play an important role in the insulating regime.

the $R_{\square}(B)$ for the wires with different w , along with the film, measured at $T=0.2 \text{ K}$. Since R_c changes with the width of the nanowires (see Table I), we normalize R_{\square} with respect to the R_c values for comparison. At $B=0$, the film has lowest R_{\square}/R_c , and $R_{\square}/R_c(B=0)$ increases gradually as we decrease the width of the wires. This changes when we re-plot the data in Figure 4(a) with a B -scale normalized with respect to respective B_c , in Figure 4(b). On both sides of B_c , R_{\square} follow a trend with

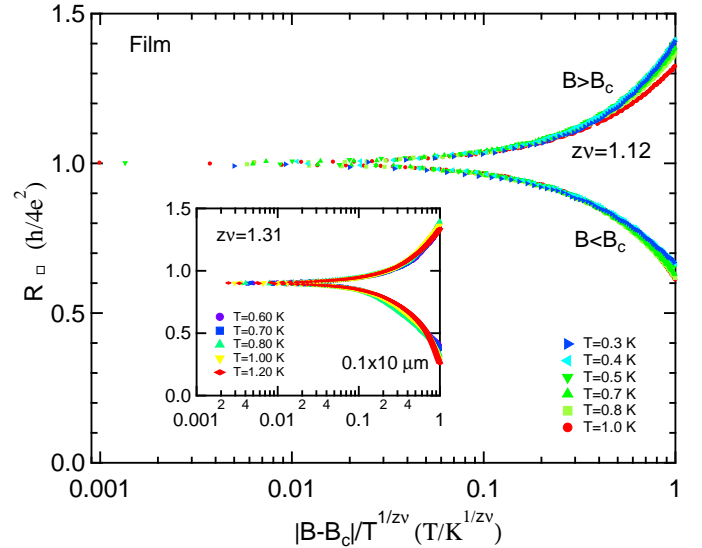


FIG. 5. Temperature scaling for the Film and $0.1 \mu\text{m}$ wide wire (inset). The shown exponent $z\nu = 1.12$ and ($z\nu=1.31$) is determined from the best visual data collapse.

size; below B_c , film has smallest R_{\square} , and it increases with the reduction in the width of nanowire, whereas for $B > B_c$, the film has more resistance and it decreases as w is reduced progressively.

The apparent linearity in the double-logarithmic representation of data as shown in Figure 4(b), for the wires along with the film, emphasize that the wires follow a similar kind of phenomenological power law behavior^{34,35}. In the superconducting side of the B -tuned SIT, the power law is consistent with the collective pinning model of transport^{22,34,36} and indicate the role played by interacting bosons (vortices) in transport. The existence of the power law behavior above B_c , suggest that vortex transport might be important in the insulating state^{34,35}.

A quantum critical point is known to separate ground states with different symmetry. Being a QPT, criticality in SIT, results in scaling laws^{1,6}. These scaling relation was obtained using the characteristic length scales, set either by T or electric field (E)⁹. It reduces to a single variable function if either of T or E is fixed. The T -scaling of R_{\square} provides the exponent $z\nu$, since the abscissa is scaled as $u = |B - B_c|/T^{z\nu}$. As a result of this T -scaling, all the curves have collapsed into one, showing at $T=0$ a bifurcation, or unstable fixed point.

For each device, $R_{\square}(B, T, E=0)$ data were used to test the scaling prediction, by varying B at small increments at fixed T . In figure 5, the T -scaling of R_{\square} for the film is shown. A good visual collapse of the data is obtained for $z\nu=1.12$, which is close to the previous findings^{6,35}. For the wires, R_{\square} flattens and become T independent on either side of B_c [figure2(b)], as low- T is approached. For obvious reason this affects the scaling. Hence, we prefer to scale wires' R_{\square} only for $T \geq 0.6 \text{ K}$. In the inset of

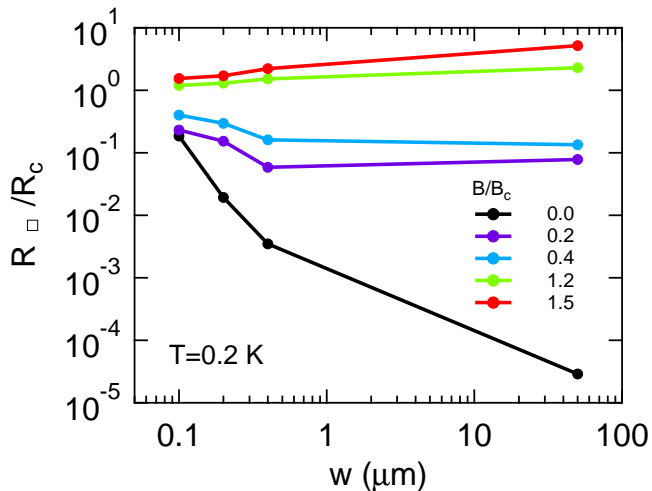


FIG. 6. The variation of R_{\square} with width (w) of wires at different $(\frac{B}{B_c})$ values measured at $T=0.2$ K. R_{\square} is normalized with respect to the respective R_c values. A log-log representation is used to include the $50 \mu\text{m}$ wide film's data in the plot. In the superconducting side of the SIT, R_{\square} decreases as w is increased, whereas, in the insulating side, R_{\square} increases with an increase in w .

figure 5, the scaling results for one of our wire devices ($0.1 \times 10 \mu\text{m}$) is shown. For the best visual collapse was obtained for $z\nu = 1.31$ which is not very different from that observed for the film. The scaling analysis near the critical point allows one to get the symmetry classification without the functional form the data follow³⁵. Although in our system the power law as shown in Figure 4, can be treated as entire scaling function.

The high- T activated behavior of R_{\square} for all the devices allows us to extract the activation energies (T_0). We find that T_0 varies logarithmically with B , following $T_0 \sim \ln(\frac{B}{B_c})$ as observed in our previous study³⁴. Theoretically, this variation of T_0 is consistent with the collective pinning model of vortex transport^{22,34,36}. This type of logarithmic field dependence of activation energy is also found in several other cases, such as thermally activated motion of vortex-antivortex pairs³⁷ or activation over surface barrier associated with edge pinning³⁸.

To show the dependence of R_{\square} on the width of the nanowires we present in Figure 6, $R_{\square}(w)$ for different $(\frac{B}{B_c})$ values measured at 0.2 K. In the superconducting side of the SIT, R_{\square} decreases as w is increased, whereas, in the insulating side, R_{\square} increases with w . A log-log representation is used to include the film's data for the same $(\frac{B}{B_c})$ values as of the wires. It is seen that the film's data follows the wires' trend as $w \rightarrow \infty$.

To illustrate the effect of size on the superconducting and insulating sides, Arrhenius plots of R_{\square} , for all the devices at same $(\frac{B}{B_c})$ values is shown in Figure 7 (a) and (b). R_{\square} was normalized with respect to respective R_c values for comparison. At high- T , the wires' R_{\square} follow the same activated form as the film, until they deviate

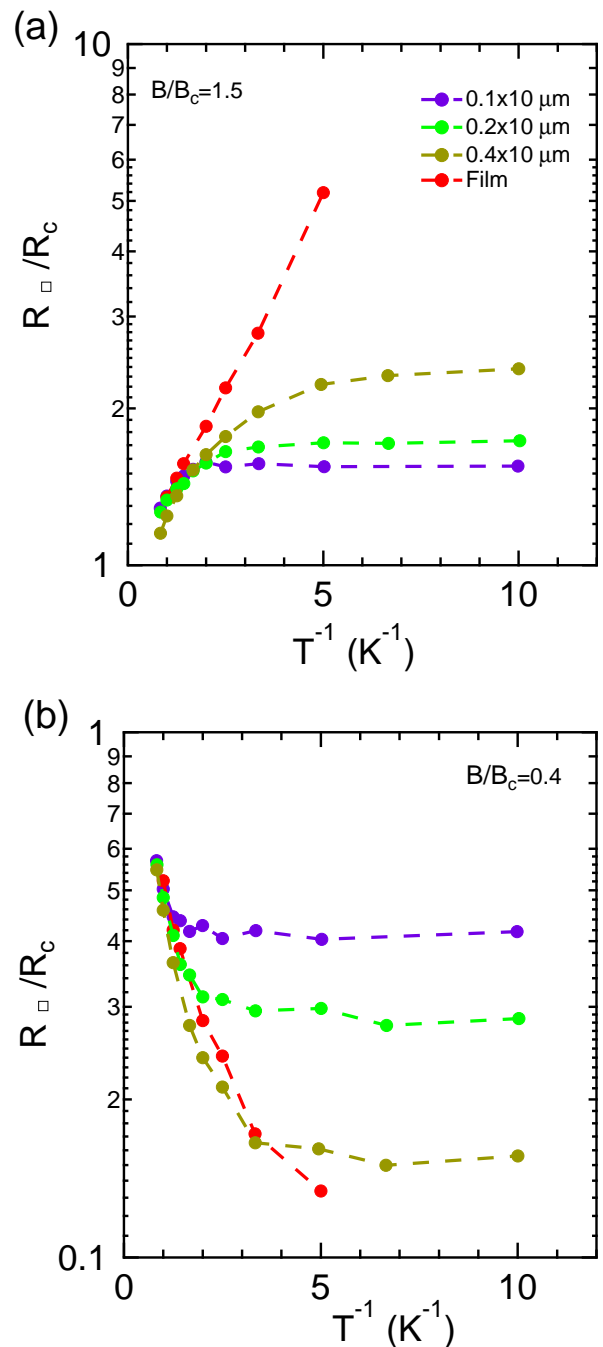


FIG. 7. Variation of normalized R_{\square} with T^{-1} for wires of different widths along with the film measured at (a) $(\frac{B}{B_c}=1.5)$ and (b) $(\frac{B}{B_c}=0.4)$. At high- T all the devices follow the same activated behavior, until the wires' R_{\square} become independent of T . Below B_c , the wire with lower w has more R_{\square} whereas, above B_c , R_{\square} increases as w is increased.

and become T -independent. The value of the saturated resistance, (R_{sat}), follows different trend with w on either side of the B -tuned SIT. In the superconducting side [as inferred from figure 7(b)], R_{sat} increases as w is reduced

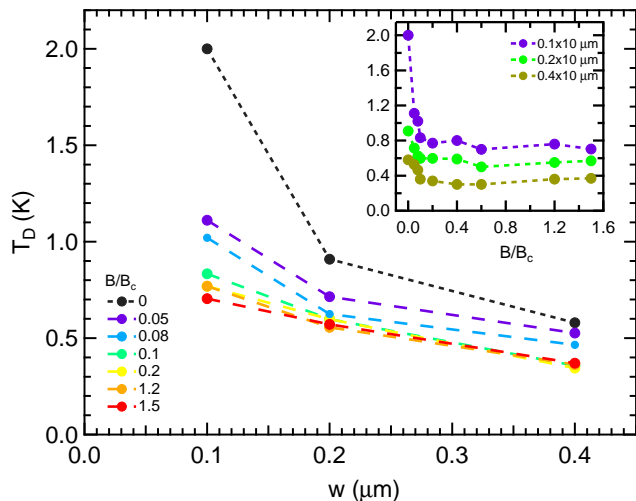


FIG. 8. Variation of temperature of deviation (T_D) (see text) with w for different $(\frac{B}{B_c})$ values. (Inset): Variation of T_D with $(\frac{B}{B_c})$ for wires with different widths. For a particular $(\frac{B}{B_c})$, T_D decreases with increase in w . For a particular w , T_D initially decreases with increasing $(\frac{B}{B_c})$ and then saturate.

whereas in the insulating side [Figure 7(a)] R_{sat} decreases with a decrease in w .

This unique width dependence of resistance in the insulating state, can be explained if we adhere to the charge-vortex duality picture of the SIT. In the superconducting phase, Cooper pairs form the superfluid condensate, whereas, vortices are localized by forming bound vortex antivortex pairs, and their motion give rise to resistance. As the channel width is reduced, the vortices can tunnel or hop from one end to another and R_{sat} is increased. On the other hand, in the insulating side, the vortex-antivortex pairs are broken by quantum fluctuations at low- T , whereas the Cooper pairs are localized and form Bose glass. The motion of these Cooper pairs would increase the conductance (reduction in resistance) in the system. Upon the reduction of the channel width, the movement of the localized Cooper pairs give lower R_{sat} in the narrower wires. This apparently leads to the fact that as we keep on decreasing the width, R_{\square} will be less in the insulating side at low- T and quasi-1D systems would never show as high R_{\square} as of 2D films over the same $(\frac{B}{B_c})$ range.

The temperature, T_D where the wires' R_{\square} deviate from the film, evolve with w and B . In Figure 8 the variation of T_D with w for different $(\frac{B}{B_c})$ values of the wire is shown. For a particular $(\frac{B}{B_c})$, T_D increases with decrease in w . For $0.4 \mu\text{m}$ wide wire, T_D is smallest of the three, as it is more close to the film, as per as dimension is concerned in comparison to the 0.2 and $0.1 \mu\text{m}$ wide wire. Also the evolution of T_D is found to have a dependence on the magnetic field, in the superconducting side, $(\frac{B}{B_c} < 1)$. In the inset of Figure. 8 the variation of T_D with $(\frac{B}{B_c})$ is shown. T_D is maximum at zero magnetic field and decreases as B is increased in the superconducting side of the B -tuned SIT, and attained saturation, which continued above B_c .

IV. SUMMARY

We performed magnetotransport measurements on several $10 \mu\text{m}$ long nanowires with different widths, along with a 2D film of a:InO. The devices showed B -driven superconductor to insulator transition. On either side of the B -driven SIT, the resistance behave differently but systematically with width. In the superconducting side, R_{\square} increases with decrease in width, whereas in the insulating side, it behaves oppositely. Initially, at high- T all of them has similar activated transport, however, as T is reduced the wires deviate from that and R_{\square} become independent of T . The temperature of deviation of wires' resistance from that of film, is found to evolve with the width of the wire and magnetic field. Our analysis suggest that at low- T , high resistance in the insulating side of SIT will be absent in narrower samples due to finite size effect on the motion of the localized Cooper pairs.

V. ACKNOWLEDGMENTS

S.M. and G.C.T. thank Sumilan Banerjee for fruitful discussions and department's sub-micron center for providing necessary support in device fabrication. S.M. thanks VATAT program for post-doctoral fellowship support. This work was supported by the Minerva Foundation with funding from Federal German Ministry for Education and Research, and by a grant from the Israel Science Foundation.

* sreemanta85@gmail.com

† dan.shahar@weizmann.ac.il

‡ Current address: Division of Physics and Applied Physics, School of Physical and Mathematical Sciences, Nanyang Technological University, Singapore 637371.

¹ S. L. Sondhi, S. M. Girvin, J. P. Carini, and D. Shahar, Rev. Mod. Phys. **69**, 315 (1997).

² S. Sachdev, *Quantum Phase Transitions*, 2nd ed. (Cambridge University Press, 1999).

³ V. F. Gantmakher and V. T. Dolgoplov, Physics-Uspekhi **53**, 1 (2010).

⁴ D. B. Haviland, Y. Liu, and A. M. Goldman, Phys. Rev. Lett. **62**, 2180 (1989).

⁵ K. A. Parendo, K. Tan, A. Bhattacharya, M. Eblen-Zayas, N. E. Staley, and A. M. Goldman, Phys. Rev. Lett. **94**,

- 197004 (2005).
- ⁶ A. F. Hebard and M. A. Paalanen, *Phys. Rev. Lett.* **65**, 927 (1990).
 - ⁷ A. M. Goldman and N. Markovic, *Phys. Today* **51**, 39 (1998).
 - ⁸ D. Shahar and Z. Ovadyahu, *Phys. Rev. B* **46**, 10917 (1992).
 - ⁹ A. Yazdani and A. Kapitulnik, *Phys. Rev. Lett.* **74**, 3037 (1995).
 - ¹⁰ T. I. Baturina, D. R. Islamov, J. Bentner, C. Strunk, M. R. Baklanov, and A. Satta, *JETP Lett.* **79**, 416 (2004).
 - ¹¹ A. T. Bollinger, G. Dubuis, J. Yoon, D. Pavuna, J. Misewich, and I. Boovi, *Nature* **472**, 458 (2011).
 - ¹² F. Sharifi, A. V. Herzog, and R. C. Dynes, *Phys. Rev. Lett.* **71**, 428 (1993).
 - ¹³ M. Zgirski, K.-P. Riikonen, V. Touboltsev, and K. Y. Arutyunov, *Phys. Rev. B* **77**, 054508 (2008).
 - ¹⁴ A. Rogachev, T.-C. Wei, D. Pekker, A. T. Bollinger, P. M. Goldbart, and A. Bezryadin, *Phys. Rev. Lett.* **97**, 137001 (2006).
 - ¹⁵ K. Arutyunov, D. Golubev, and A. Zaikin, *Phys. Rep.* **464**, 1 (2008).
 - ¹⁶ A. Johansson, G. Sambandamurthy, D. Shahar, N. Jacobson, and R. Tenne, *Phys. Rev. Lett.* **95**, 116805 (2005).
 - ¹⁷ G. Sambandamurthy, L. W. Engel, A. Johansson, and D. Shahar, *Phys. Rev. Lett.* **92**, 107005 (2004).
 - ¹⁸ G. Sambandamurthy, L. W. Engel, A. Johansson, E. Peled, and D. Shahar, *Phys. Rev. Lett.* **94**, 017003 (2005).
 - ¹⁹ N. Mason and A. Kapitulnik, *Phys. Rev. Lett.* **82**, 5341 (1999).
 - ²⁰ Y. Qin, C. L. Vicente, and J. Yoon, *Phys. Rev. B* **73**, 100505 (2006).
 - ²¹ Y.-H. Lin, J. Nelson, and A. M. Goldman, *Phys. Rev. Lett.* **109**, 017002.
 - ²² D. Ephron, A. Yazdani, A. Kapitulnik, and M. R. Beasley, *Phys. Rev. Lett.* **76**, 1529 (1996).
 - ²³ W. Liu, L. Pan, J. Wen, M. Kim, G. Sambandamurthy, and N. P. Armitage, *Phys. Rev. Lett.* **111**, 067003 (2013).
 - ²⁴ J. M. Graybeal, P. M. Mankiewich, R. C. Dynes, and M. R. Beasley, *Phys. Rev. Lett.* **59**, 2697 (1987).
 - ²⁵ H. Kim, S. Jamali, and A. Rogachev, *Phys. Rev. Lett.* **109**, 027002 (2012).
 - ²⁶ M. P. A. Fisher, *Phys. Rev. Lett.* **65**, 923 (1990).
 - ²⁷ A. Ghosal, M. Randeria, and N. Trivedi, *Phys. Rev. B* **65**, 014501 (2001).
 - ²⁸ Y. Dubi, Y. Meir, and Y. Avishai, *Nature* **449**, 876 (2007).
 - ²⁹ N. Giordano, *Phys. Rev. Lett.* **61**, 2137 (1988).
 - ³⁰ M. Ovadia, B. Sacépé, and D. Shahar, *Phys. Rev. Lett.* **102**, 176802 (2009).
 - ³¹ M. Ovadia, D. Kalok, I. Tamir, S. Mitra, B. Sacépé, and D. Shahar, *Sci. Rep.* **5**, 13503 (2015).
 - ³² B. Spivak and F. Zhou, *Phys. Rev. Lett.* **74**, 2800 (1995).
 - ³³ J. A. Chervenak and J. M. Valles, *Phys. Rev. B* **61**, R9245 (2000).
 - ³⁴ G. Sambandamurthy, A. Johansson, E. Peled, D. Shahar, P. G. Björnsson, and K. A. Moler, *Euro. Phys. Lett.* **75**, 611 (2006).
 - ³⁵ M. Ovadia, D. Kalok, B. Sacepe, and D. Shahar, *Nat Phys.* **9**, 415 (2013).
 - ³⁶ G. Blatter, M. V. Feigel'man, V. B. Geshkenbein, A. I. Larkin, and V. M. Vinokur, *Rev. Mod. Phys.* **66**, 1125 (1994).
 - ³⁷ H. J. Jensen, P. Minnhagen, E. Sonin, and H. Weber, *Euro. Phys. Lett.* **20**, 463 (1992).
 - ³⁸ A. Koshelev, *Physica C: Superconductivity* **223**, 276 (1994).